water

MDPI

*Article*

# Optimization of Critical Factors Affecting Dynamic Membrane Formation in a Gravity-Driven Self-Forming Dynamic Membrane Bioreactor towards Low-Cost and Low-Maintenance Wastewater Treatment

**Luhe Tang [1], Jingyu Zhang [1], Lulu Zha [2,3], Yisong Hu [2,3,*], Yiming Yang [1], Yunsheng Zhao [1], Xinglong Dong [1], Zhanjiu Wang [1], Weihang Deng [2,3] and Yuan Yang [2,3]**

[1] Beijing Huayu Brilliant Eco-Environmental Protection Technology Co., Ltd., Beijing 102412, China; tang_1680@126.com (L.T.); zhangjingyu@huayuhuihuang.cn (J.Z.); 15811321317@126.com (Y.Y.); shang_lisi@163.com (Y.Z.); dongxinglong163@163.com (X.D.); wzjayh9@163.com (Z.W.)
[2] Shanxi Key Laboratory of Environmental Engineering, Xi'an University of Architecture and Technology, Xi'an 710055, China; cll01070204@163.com (L.Z.); yuanyang@xauat.edu.cn (Y.Y.)
[3] Key Lab of Northwest Water Resource, Environment and Ecology, MOE, Xi'an University of Architecture and Technology, Xi'an 710055, China
* Correspondence: huyisong@xauat.edu.cn; Tel.: +86-029-8220-5652

**Abstract:** Self-forming dynamic membrane (SFDM) formation is affected by a variety of operating conditions. However, previous studies have only focused on individual influencing factors and a systematic analysis of important factors is lacking. In this study, an aerobic self-forming dynamic membrane bioreactor (SFDMBR) was developed for the treatment of domestic wastewater with the critical factors that affect the effective formation of SFDM optimized, and the operational performances under optimized formation conditions confirmed. The results indicated that SFDM could be formed within 5 min using 48 μm stainless-steel mesh as the supporting material at a sludge concentration of 5–6 g/L and a gravity waterhead of 15 cm. And the SFDM formed could maintain a stable flux of 30–50 LMH, and the removals of COD, SCOD, and $NH_4^+$-N were 93.28%, 82.85%, and 95.46%, respectively. Furthermore, the cake layer resistance (reversible fouling) contributed to 95.93% of the total filtration resistance, thus a simple physical cleaning can effectively restore the flux indicating a low-maintenance requirement. This study provides valuable insights into the optimization and application of the SFDMBR process.

**Keywords:** self-forming dynamic membrane bioreactor; domestic wastewater; operational conditions; pollutants removal; filtration resistance

check for updates

**Citation:** Tang, L.; Zhang, J.; Zha, L.; Hu, Y.; Yang, Y.; Zhao, Y.; Dong, X.; Wang, Z.; Deng, W.; Yang, Y. Optimization of Critical Factors Affecting Dynamic Membrane Formation in a Gravity-Driven Self-Forming Dynamic Membrane Bioreactor towards Low-Cost and Low-Maintenance Wastewater Treatment. *Water* **2023**, *15*, 3963. https://doi.org/10.3390/w15223963

Academic Editor: Jesus Gonzalez-Lopez

Received: 5 October 2023
Revised: 3 November 2023
Accepted: 13 November 2023
Published: 15 November 2023

**Copyright:** © 2023 by the authors. Licensee MDPI, Basel, Switzerland. This article is an open access article distributed under the terms and conditions of the Creative Commons Attribution (CC BY) license (https://creativecommons.org/licenses/by/4.0/).

## 1. Introduction

Membrane bioreactors (MBRs) technology, combining the membrane separation with biological treatment, is a cost-effective alternative for wastewater treatment [1,2]. Due to its complete solid retention, superior effluent quality, compact footprint, and selective control over hydraulic retention time (HRT) and sludge retention time (SRT), the MBR technology has been extensively used in the treatment of municipal and industrial wastewater [3–5]. However, membrane fouling caused by the complex interactions between various foulants and membrane materials reduces process efficiency, shortens membrane lifespan, and increases operational costs [6,7].

The dynamic membrane bioreactor (DMBR) has garnered significant interest recently due to its ability to address the low flux and easy fouling limitation related to the MBR [8–10]. Dynamic membrane (DM) refers to the second membrane formed on the supporting material when filtering solution contains suspended particles [11]. The primary difference between the supporting material used in the development of a DM and

a conventional membrane is membrane pore size, which ranges between 10 and 200 μm and 0.1–1.0 μm in the DMBR and MBR. Higher filtration flux, ease of cleaning, and cost-effectiveness make the DMBR increasingly competitive for wastewater and organic wastes management with the assistance of various coarse-pore supporting materials [12]. Based on the distinction in DM formation, DM can be classified as self-forming dynamic membranes (SFDMs) or precoated dynamic membranes (PCDMs) [13]. PCDM is formed by pre-filtering a solution containing one or more colloidal components through the supporting material [12,14,15]; SFDM is created when organic matter, colloids, and suspended solids in the sludge mixture are naturally deposited on the surface of the supporting material during the filtration process. SFDM is more promising than PCDM for wastewater treatment since PCDM requires additional pre-coating chemical and pre-coating process, which raises the difficulties of practical application.

The development of a stable and resilient DM is a necessity for the removal of pollutions from SFDMBR, as the well-formed cake layer is the only factor that influences this process [16]. However, several variables, including pore size and supporting material, sludge concentration, and driving force (waterhead in gravity-driven filtration mode), play an important role in the formation and steady operation of SFDM. Based on previous studies, larger pore sizes of supporting material is known to lengthen the period that SFDM production occurs (a process that results in low-quality effluent), but smaller ones causes serious membrane fouling [17,18]. Sabaghian et al. [19] reported that the formation of DM took 120 min, 80 min, 40 min, and 5 min at sludge concentrations of 3 g/L, 5 g/L, 7 g/L, and 9 g/L. And another study also reported that high concentration of MLSS contributed to the rapid formation of DM [20]. One study showed that a gravity waterhead of 70 mm promotes the rapid formation of SFDM and eliminates the enrichment of excess sludge on the cake layer under high pressure [14]. Therefore, realizing rapid formation followed by a stable operation of the SFDM by adjusting aforementioned parameters is crucial for the development of SFDMBR. However, as known, the effects of a specific operating condition on SFDM formation have been reported, but there is a lack of systematic analysis and optimization of important factors to realize the rapid formation of SFDM and reduce the membrane cleaning requirement.

Therefore, this study established a lab-scale gravity-driven SFDMBR to systematically investigate the effects of supporting material, membrane pore size, sludge concentration, and gravity waterhead on SFDM formation and stable operation. The study also discussed the filtration performance, pollutant removal, and properties of the SFDM under optimized operational conditions. The results are expected to provide technical support for SFDMBR wastewater treatment technology.

## 2. Materials and Methods

### *2.1. Wastewater, Sludge Inoculation and Supporting Materials*

The SFDMBR was fed with the real domestic wastewater collected from the inlet of a local wastewater treatment plant (WWTP) in Xi'an, China. The influent had a total chemical oxygen demand (COD) of 526.73 ± 62.57 mg/L and soluble COD (SCOD) of 188.67 ± 9.75 mg/L, an ammonia nitrogen ($NH_4^+$-N) of 46.57 ± 2.95 mg/L, a total nitrogen (TN) of 62.41 ± 3.07 mg/L, a total phosphorus (TP) 6.78 ± 0.65 mg/L, with the turbidity of 148 NTU on average during the operation period. The activated sludge for inoculation was taken from the aerobic tank in the same WWTP adopting anaerobic-anoxic-oxic-MBR (AAO-MBR) process. The mixed liquor suspended solids (MLSS) used in the batch experiments were controlled at 3–4 g/L, 5–6 g/L, and 7–8 g/L, respectively, which were thickened by gravity concentration and acclimated for two weeks before use. The supporting materials used for SFDM formation were stainless steel mesh (pore size of 75, 48, and 25 μm), polyester (pore size of 75 μm), screen silk (pore size of 75 μm), nylon mesh (pore size of 75 μm), and non-woven fabric (specific weight of 120 g/$m^2$).

### *2.2. Experimental Setup and Operation Conditions*

#### 2.2.1. Reactor Setup and Operation

The lab-scale SFDMBR with a working volume of 9.8 L was established in the local WWTP, with the schematic shown in Figure 1a. Two self-fabricated, flat-sheet SFDM modules were symmetrically submerged in the bioreactor, each having an effective filtering area of 0.02 $m^2$. As shown in Figure 1b, the self-fabricated flat-sheet SFDM module was constructed with plexiglass for the frame, a grid-shaped, highly pressure-resistant stainless-steel bracket for internal support, and corresponding membrane material wrapped externally to create the appearance of a box with an interior cavity. The aeration system was installed in the bottom of the bioreactor to provide shear force across the membrane and dissolved oxygen (DO). Bottom aeration was regulated through gas flowmeter to provide DO requirements for microorganisms at 2–5 mg/L. The influent was pumped into the bioreactor through a peristaltic pump (Longer BT-100, Baoding, China), and a controller (JYB-714, Wenzhou, China) was connected to the influent pump to maintain a relatively stable water level. Continuous effluent was obtained under the gravity waterhead differences between the water level and the outlet in bioreactor. The operating temperature was maintained at 25 ± 1 °C

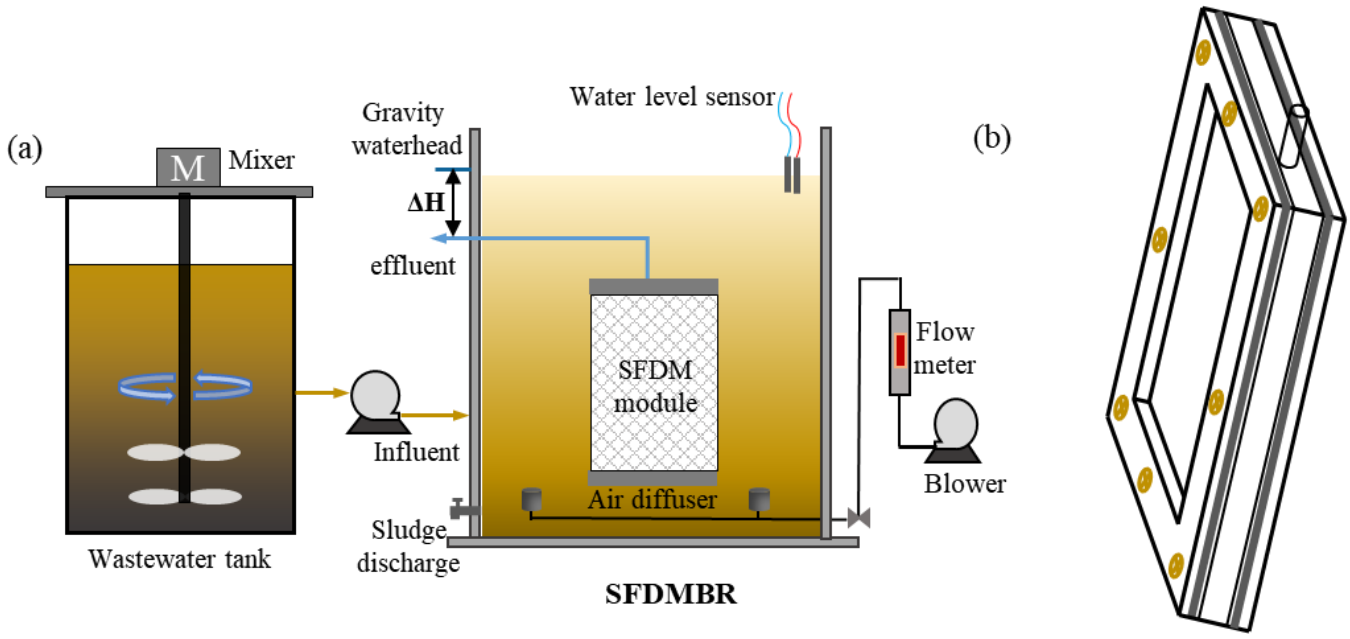


**Figure 1.** The schematic diagram of the SFDMBR; and SFDM module: (**a**) SFDMDR; (**b**) SFDM module.

#### 2.2.2. Batch Filtration Tests for Efficient SFDM Formation

To maximize the SFDM formation conditions, a series of batch experiments based on single factor analysis and the control variable method (CVM) were developed. The four stages of the batch filtering experiments were membrane pore size optimization, sludge concentration optimization, gravity head optimization, and supporting material optimization. Firstly, as for the supporting materials, five distinct membrane materials (stainless steel mesh, polyester, silk sieve, nylon mesh, and non-woven fabric) were chosen. One membrane material was then ideally chosen based on the filtration performance, while other conditions are maintained as follows: a 75 μm membrane pore size, 3–4 g/L of sludge concentration, and a 10 cm gravity waterhead. Subsequently, the membrane pore sizes (75 μm, 48 μm, and 25 μm) were altered based on the favored supporting material. Based on pollutants removal and filtration performances, the ideal pore size was selected. Afterwards, the sludge concentration was varied (3–4 g/L, 5–6 g/L, and 7–8 g/L) based on the constant supporting material and membrane pore size, and the optimal sludge

concentration was determined based on the filtration performance and pollutants removal. Finally, to optimize the gravity waterhead, the process performance the SFDMBR was compared under various gravity waterheads (10 cm, 20 cm, and 30 cm). For each batch filtration test, a fresh membrane module was used, and the filtration time was set to 24 h to guarantee the correctness of the results.

#### 2.2.3. Continuous Operation of the SFDMBR

Following batch tests, the SFDMBR was operated for five continuous filtration cycles under optimal operating conditions. The filtration cycle was set for 48 h, and at the end of each cycle the mesh was physically cleaned by air back-flushing (2 min with an air flow rate of 75 L/min) plus surface brushing (2 min) according to our previous work [21]. With the exception of sampling for sludge characteristics study, no sludge was released, indicating an infinite SRT. To keep the DO concentration between 2 and 5 mg/L, the aeration intensity was set to 2 L/min.

### *2.3. Analytical Methods*

#### 2.3.1. Water Sample Collection and Measurement

Water samples were collected at the end of each batch filtration experiment and at the end of each operational cycle (48 h). SCOD and $NH_4^+$-N was detected after samples filtrating through 0.45 μm filters. COD, SCOD, $NH_4^+$-N, TN, TP, MLSS, and mixed liquor volatile suspended solids (MLVSS) were determined according to the standard methods [22]. The filtration flux (J, L/$m^2$h, LMH) of the SFDM was calculated by measuring the permeate volume ($\Delta v$, L) collected during a specified time interval ($t$, h) and a given membrane area ($A$, 0.02 $m^2$) ($J = \frac{\Delta V}{A\,t}$). The turbidity of influent and effluent was conducted with a turbidity meter (TB 211 IR, Lovibond, German), DO was detected by using a DO meter (JPBJ-608, Shanghai, China), and pH was measured using a portable pH meter (PHS-3C, Shanghai, China).

#### 2.3.2. SFDM Properties Analysis

The membrane module was carefully removed from the bioreactor, and then the SFDM was collected for further analysis at the end of a long-term filtration period according to the previous studies [23]. In detail, the SFDM layer was scraped off by a plastic sheet and transferred to a measuring cylinder containing pure water. The average thickness was calculated according to the volume difference. In addition, the morphology and inorganic elements of pre-treated SFDM were analyzed using a scanning electron microscope (SEM, Quanta650FEG, FEI, USA) connected to an energy-dispersive X-ray analyzer (EDX, Quanta650FEG, FEI, USA).

Another SFDM module was used to determine the filtration resistance distribution by the following equation (Darcy's Law) [16,24].

$$R_t = R_m + R_c + R_p = \Delta P/\mu$$

$$R_c = R_t - R_m - R_p$$

where $R_t$ is the total resistance of the SFDM layer ($m^{-1}$); $R_m$ is the intrinsic resistance of the stainless steel mesh ($m^{-1}$), which was measured as the new membrane module in pure water; $R_c$ is the cake layer resistance ($m^{-1}$), which can be obtained by subtracting the filtration resistance of $R_m$ and $R_p$ from $R_t$; $R_p$ is the pore blocking resistance ($m^{-1}$), calculated by subtracting $R_m$ from $R_t$ after air back-flushing plus surface brushing; $\Delta P$ is the gravity waterhead induced hydrodynamic pressure; $\mu$ is the viscosity of the permeate (Pa·s); and $J$ is the filtration flux (m/s).

2.3.3. Statistical Analysis

The IBM SPSS Statistics 25.0 software (international Business Machines Co., Armonk, NY, USA) was used for statistical analysis. Specifically, the average values and standard deviations (±SD) were determined. Graphics and error bars were drawn using Origin2021 software.

## 3. Results and Discussion

### *3.1. Optimization of SFDM Supporting Material*

Selection of an appropriate supporting material enabling the formation of a DM is a critical step for SFDMBR application. For the batch filtration tests, stainless steel mesh, nylon mesh, polyester, silk sieve (pore size of 75 μm), and 120 g/m$^2$ non-woven fabric were chosen as the supporting materials. Variation in filtration flux and effluent turbidity using different supporting materials were shown in Figure 2. Initial filtration flux of stainless-steel mesh, nylon mesh, sieve silk, polyester, and non-woven fabrics was 585, 456, 498, 420, and 777 LMH. The filtration flow decreased to 192, 207, 195, 195, and 297 LMH after five minutes later, respectively. The filtration flux of the five supporting materials was attenuated to about 40% of the initial fluxes in the first 5 min, indicating the formation of SFDM layer on the mesh surface and decrease in filtration flux along with the operation time. Afterwards, the decreasing rates of flux slowed down, as the stable flux at the end of operation for the five supporting materials was 33, 27, 33, 30, and 36 LMH, respectively.

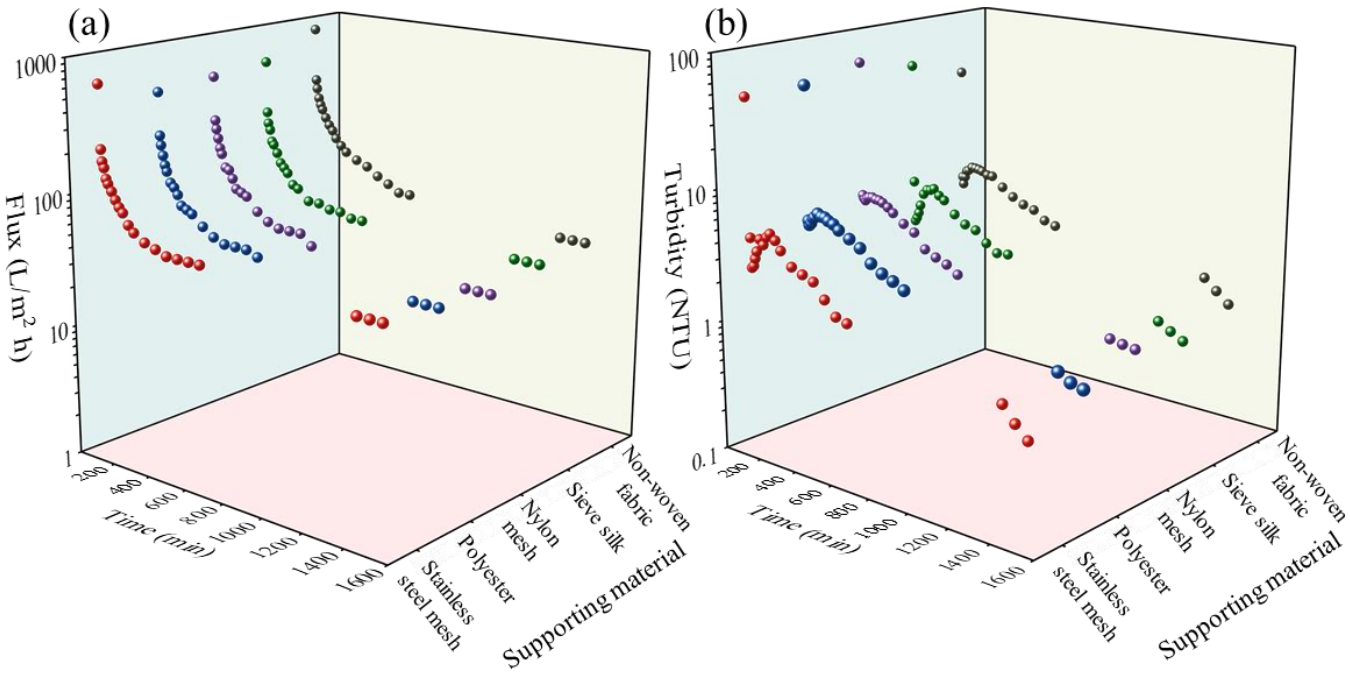


**Figure 2.** Filtration performance using different supporting materials (stainless steel mesh, polyester, nylon mesh, silk sieve and non-woven fabric): (**a**) filtration flux and (**b**) effluent turbidity. Each circle corresponds to each horizontal coordinate in the 3D plot.

The trend of effluent turbidity altered in agreement with the flux, as shown in Figure 2b (fast drop to stabilization). The influent turbidity varied between 140 and 170 NTU; however, the effluent turbidity of the five membrane materials decreased dramatically after 5 min to 3.78, 4.76, 4.75, 3.89, and 4.08 NTU, respectively. According to the previous studies [20,21,23], it was reported that effluent turbidity below 5 NTU was defined as an indicator of SFDM formation, thus five supporting materials could form SFDM within 5 min. The effluent turbidity after SFDM formation was relatively stable, and decreased slowly with the filtration time. When the effluent turbidity was reduced to less than 2 NTU,

it represented the formation of stabilized SFDM [25]. Therefore, for stainless steel mesh, nylon mesh, sieve silk, and polyester, 7 h was noted for effluent turbidity declining below 2 NTU and longer time for non-woven fabric.

Stainless steel mesh, silk sieve, and non-woven fabric had greater stable flux. However, non-woven fabric took longer to generate stable SFDM and was more difficult to clean. Stainless steel mesh was chosen as the supporting material for effective SFDM construction because it had a solid structure that could sustain the necessary pressure for an extended period of time and could be reused after membrane cleaning.

### 3.2. Optimization of Membrane Pore Size

Large pore size supporting material might worsen the quality of the effluent during the startup phase or following membrane cleaning. Additionally, it took them a fair amount of time to create an efficient SFDM. However, membrane fouling requires frequent membrane cleaning for the supporting material with smaller pore size. As a result, the supporting material should have an appropriate pore size to balance SFDM formation and membrane fouling.

As shown in Figure 3a,b, using stainless steel mesh with different pore size (75 μm, 48 μm, and 25 μm) as the supporting materials, the filtration flux, and effluent turbidity were measured to further explore the effect of pore size on SFDM formation. Initially, there were 585, 515, and 450 LMH in the 75, 48, and 25 μm stainless steel mesh, respectively. Afterwards, 25 μm stainless steel mesh tended to be blocked by sludge particles, causing a faster decrease in the filtration flux. The benefit of high flux operation was lost for the SFDMBR when the filtration flux of 25 μm stainless steel mesh dropped to 18 LMH at the conclusion of operation; however, for 75 and 48 μm stainless steel mesh, the filtration flux at the conclusion of a 24 h operation was 33 and 33 LMH, respectively. Thus, membrane fouling was significantly lower than 25 μm stainless steel mesh, which is consistent with other findings [17,18]. It is noteworthy that the SFDM formation time could be shortened for smaller pore size, as evidenced by the fact that 75 μm stainless steel mesh required 120 min to achieve effluent turbidity lower than 2 NTU (defined as an indicator of stable SFDM formation), whereas 48 and 25 μm stainless steel mesh required 80 and 50 min, respectively [14,26]. Following stable SFDM formation, no discernible variation in effluent turbidity was noted for varying pore sizes.

The COD and SCOD removal of stainless-steel mesh with different pore sizes (75 μm, 48 μm, and 25 μm) were shown in Figure 3c. For three membrane pore sizes of stainless-steel mesh, the influent COD was 242.95, 303.7, and 288.35 mg/L, while the influent SCOD was 149.8, 92.74, and 96.78 mg/L, in that order. Moreover, 51.98, 35.61, and 34.95 mg/L of COD and 48.97, 35.09, and 33.75 mg/L of SCOD were found in the effluent. The effluent COD from the 75 μm stainless steel mesh was significantly greater than that of the other meshes; however, Sahinkaya [10] and Meng [27] reported the effluent COD was not affected by pore size after SFDM formation. This might be explained by the fact that the SFDM performed a poor job of retaining SCOD, and the high SCOD concentration in the influent during the batch tests conducted with 75 μm stainless steel mesh. Thus, considering the stable flux, SFDM formation time, and COD removal, 48 μm was regarded as the most suitable pore size for SFDM formation.

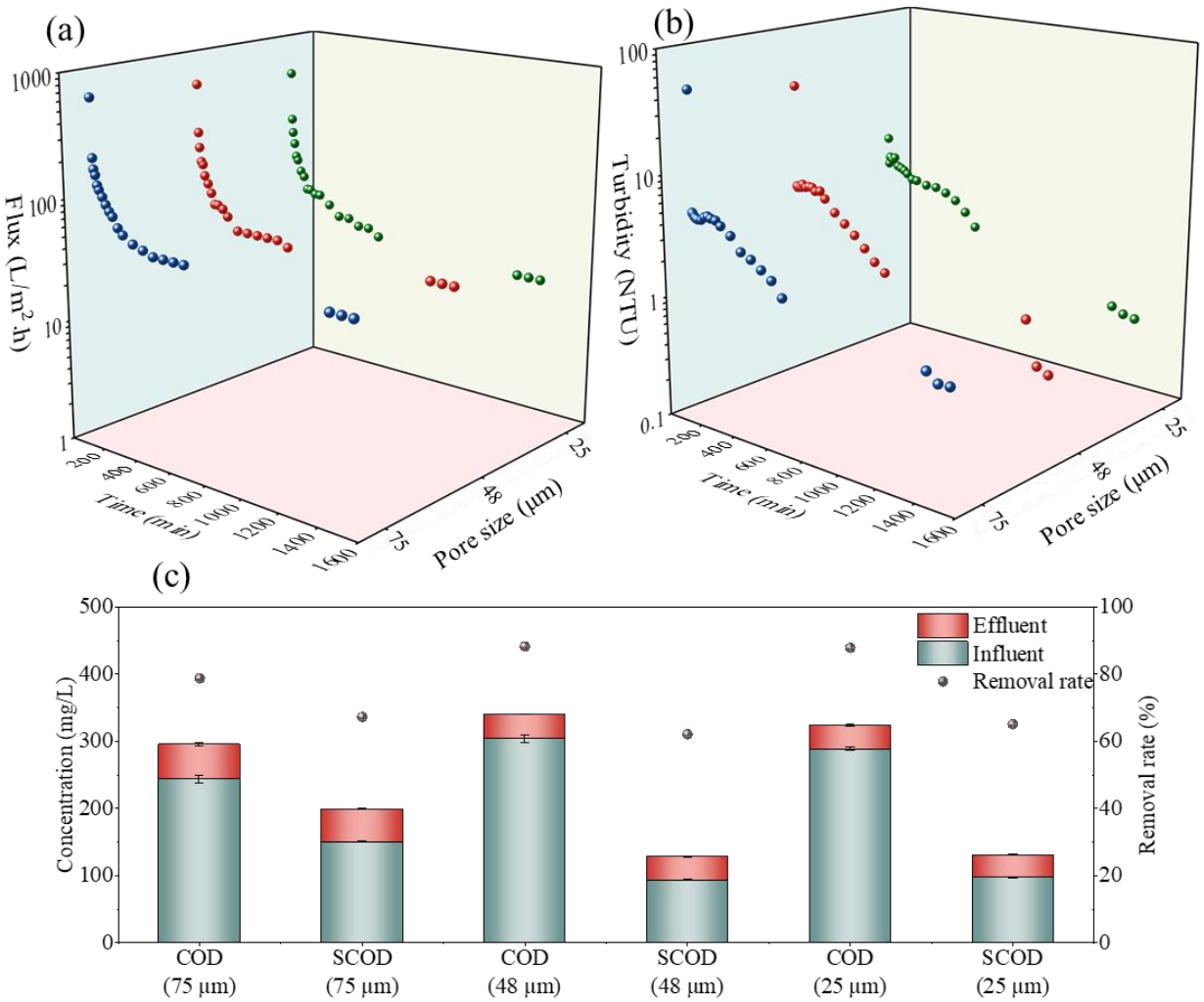


**Figure 3.** Filtration performance and COD removal under different mesh pore sizes (75, 48, and 25 μm): (**a**) filtration flux; (**b**) effluent turbidity; (**c**) COD and SCOD removal.

### *3.3. Optimization of MLSS Concentration*

The filtration flux in the SFDMBR at MLSS concentrations of 3–4 g/L, 5–6 g/L, and 7–8 g/L was shown in Figure 4a. The initial flux of the SFDMBRs was 507, 303, and 204 LMH, respectively. Due to the rapid deposition of sludge particles on the stainless-steel mesh, the filtration flux rapidly decreased to 162, 147, and 132 LMH within 5 min. Afterwards, the decreasing rate of filtration flux slowed down along with the operation time, as the filtration flux dropped to 27, 24, and 15 LMH at end of operation. The filtration flux was significantly lower at 7–8 g/L MLSS concentration in comparison to those of 3–4 g/L and 5–6 g/L MLSS concentration. As the MLSS concentration increased, more particles would be further deposited on the DM layer; as a result, membrane pore size was blocked causing the decrease in filtration flux [28,29]. As shown in Figure 4b, the initial turbidity of the SFDMBR was 21.5, 29.9, and 14.8 NTU, respectively. All of them could be reduced to less than 5 NTU in 5 min. However, the initial formation of the SFDM was not stable, the effluent turbidity was influenced by aeration in the SFDMBR. The effluent turbidity fluctuated from 2.88 NTU to 4.53 NTU at 3–4 g/L MLSS concentration; however, there was no obvious fluctuation of effluent turbidity at higher MLSS concentration (5–6 g/L and 7–8 g/L), showing that the formation of SFDM with higher sludge concentration was more stable, and the ability to resist hydrodynamic disturbance. A total of 150, 30 and 20 min was required for SFDM formation at different MLSS concentrations (3–4 g/L, 5–6 g/L, and 7–8 g/L). However, the stable effluent turbidity of the SFDMBR was not the lowest

at the high MLSS concentration (7–8 g/L), which may be due to the increased dynamic membrane thickness and the permeation of small particles into the effluent under higher hydraulic pressure [25].

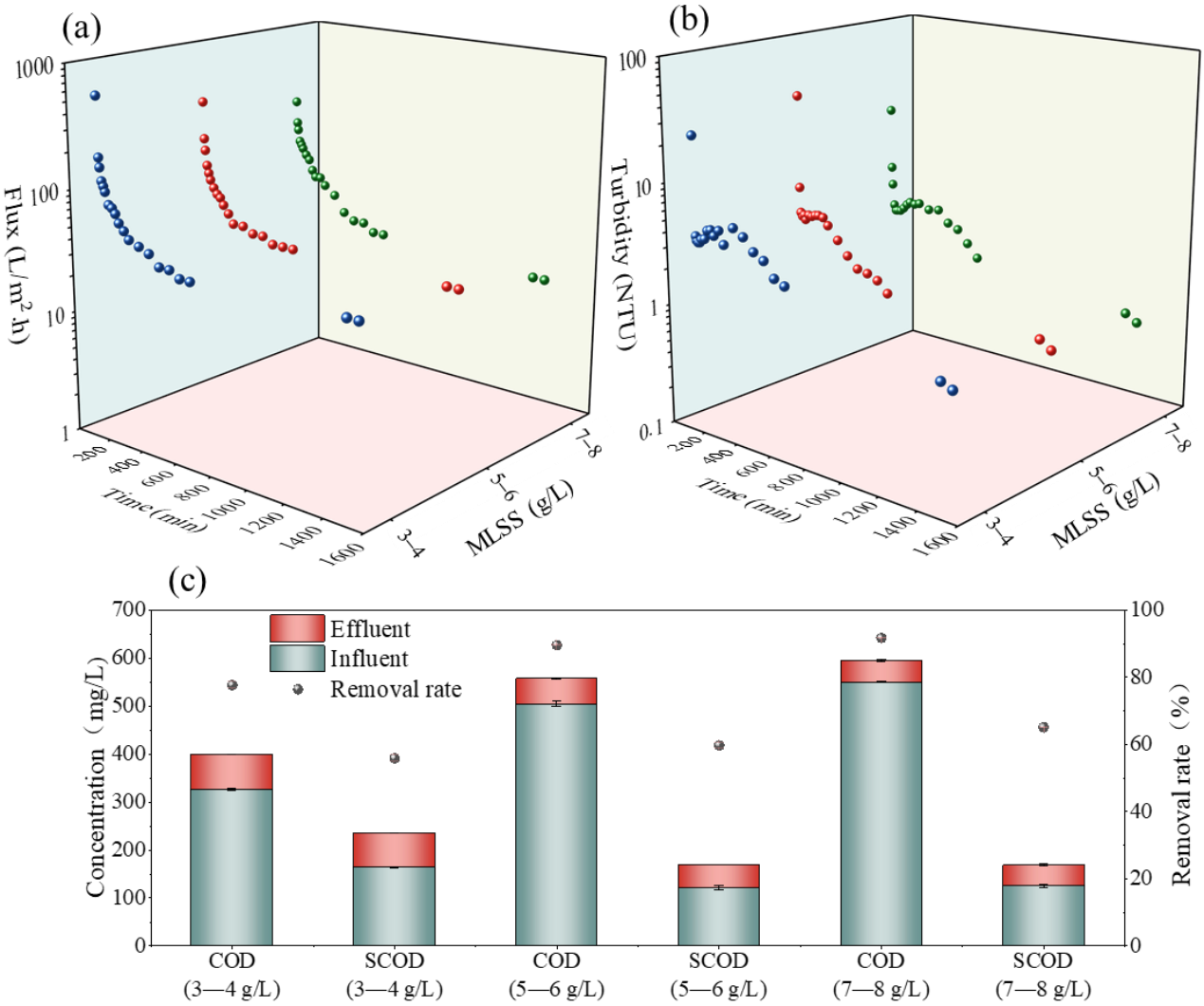


**Figure 4.** Filtration performance and COD removal under different MLSS concentrations (3–4, 5–6 and 7–8 g/L): (**a**) filtration flux; (**b**) effluent turbidity; (**c**) COD and SCOD removal.

As shown in Figure 4c, influent COD fluctuated between 320 and 550 mg/L, and the SCOD was in the range of 100–170 mg/L. At the end of operation, effluent COD at three different sludge concentrations was 72.61 (3–4 g/L), 52.37 (5–6 g/L), and 45.31 mg/L (7–8 g/L); effluent SCOD was 72.01, 48.44, and 43.35 mg/L, respectively. The corresponding COD removal was 77.71%, 89.61%, and 91.75%, and the SCOD removal was 55.89%, 55.88%, and 65.17%, respectively. On the one hand, as the MLSS concentration increased, more COD could be degraded by abundant microorganisms. On the other hand, the SFDM layer formed under high MLSS concentration was more denser, so more COD was retained and degraded, which was in agreement with previous studies reported that sludge concentration below 5 g/L resulted in inadequate biodegradation [30,31].

In summary, the MLSS of 5–6 g/L concentration was more preferable to promote efficient SFDM formation because of the shorter duration for SFDM formation, the reduced propensity for pore blockage, as well as the stable and robust in dynamic membrane structure.

### *3.4. Optimization of Gravity Waterhead*

As seen in Figure 5a, the filtration flux of SFDM in various gravity waterheads, including 10 cm, 20 cm, and 30 cm was examined. With the gravity waterhead increasing from 10 cm to 30 cm, the initial flux increased from 303 LMH to 660 LMH, indicating that hydrodynamics had a major role in determining the initial flux prior to SFDM formation. The highest flux decreased was observed at 30 cm waterhead, as the filtration flux at the 30 cm gravity waterhead decreased to 147 LMH after 5 min; however, which decreased to 162 LMH at 20 cm gravity waterhead. At the end of the 24 h operation, the filtration flux under the three gravity waterhead dropped to 18, 21 and 15 LMH, respectively, so it was obvious that there was no direct correlation between the gravity waterhead and the stable flux after the formation of SFDM. This might be due to the strong compaction effect of the greater waterhead on the SFDM, resulting in an increase in the DM thickness and pore-clogging propensity, and a decrease in the membrane porosity [32,33].

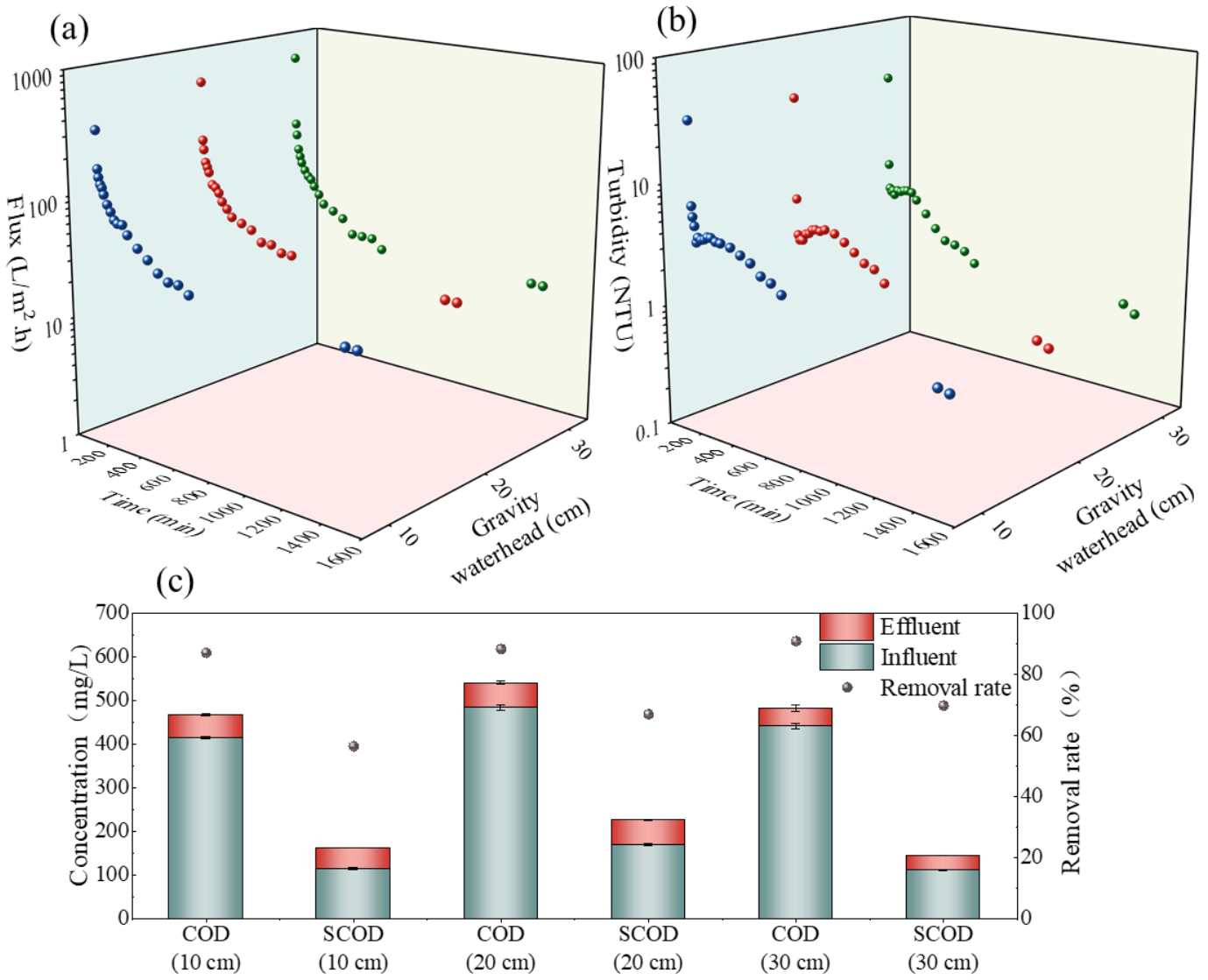


**Figure 5.** Filtration performance and COD removal under different gravity waterheads (10, 20, and 30 cm): (**a**) filtration flux; (**b**) effluent turbidity; (**c**) COD and SCOD removal.

As shown in Figure 5b, initial effluent turbidity was 29.4, 31.0, and 29.9 NTU at 10, 20 and 30 cm gravity waterhead, respectively. A total of 10, 5, and 3 min was required for effluent turbidity decreasing below 5 NTU, respectively, suggesting that SFDM formation was accelerated under higher gravity waterhead. In addition, the effluent turbidity under high gravity waterhead lose was significantly decreased at the initial stage (the initial effluent turbidity under 30 cm waterhead is lower than those of 20 and 10 cm) due to the compaction and thickening of the DM. The COD and SCOD removal at different gravity waterhead were shown in Figure 5c. The COD removal under three gravity waterhead was 87.08%, 88.31%, and 90.82%, and the SCOD removal was 56.50%, 66.96%, and 69.77%, respectively. The removal efficiency of SCOD at 20 cm and 30 cm gravity waterhead was significantly higher than that at 10 cm, which might be due to the fact that the more stable the SFDM structure formed under the higher waterhead [34,35].

Based on the filtration performance and COD removal, it can be concluded that the gravity waterhead for efficient SFDM formation was between 10 and 20 cm, thus gravity waterhead of 10, 15, and 20 cm were selected and operated for 3 d to further determine the optimum gravity waterhead. As shown in Figure 6, consistent with the results of the above tests, the filtration flux was positively related to the gravity waterhead in the initial stage. But after the SFDM formation, the filtration flux at the end of the 3 d operation decreased to 24 LMH at 15 cm gravity waterhead, and the filtration flux was 15 LMH and 12 LMH at 20 cm and 10 cm gravity waterhead, indicating that the SFDM layer was severely consolidated at greater waterhead causing the decrease in the porosity and filtration flux. The effluent turbidity during the initial SFDM formation stage was lowest at 20 cm gravity waterhead; however, the effluent turbidity during the stabilization stage was lowest at 15 cm gravity waterhead. This might because that the rate of SFDM formation increased during the initial stage at high waterhead, and therefore the turbidity decreased at a faster rate; however, after stabilization of the SFDM formation, too many particles escaped through the DM into the effluent under 20 cm waterhead. The influent COD at 10, 15, and 20 cm gravity waterhead was 481.11, 574.71, and 536.73 mg/L, and the effluent COD was 41.96, 40.33, and 36.67 mg/L, and the COD removal rate was 91.26%, 92.97%, and 93.17% on average. To sum up, 15 cm was finally selected as the optimal gravity waterhead for SFDM formation under the operational conditions in this work.

### *3.5. Long-Term Process Performance of the SFDMBR*

#### 3.5.1. Filtration Performance

The filtration flux and effluent turbidity of during five consecutive operation cycles of the SFDMBR under optimized condition (48 μm stainless steel mesh, 5–6 g/L MLSS concentration and 15 cm gravity waterhead) were shown in Figure 7. The constant pressure filtration mode driven by an average gravity waterhead of 15 cm resulted in a gradual decrease in the filtration flux. The initial flux varied between 401 and 428 LMH during five consecutive filtration cycles. Then, after 5 min the filtration flux was quickly reduced to 148–192 LMH, consistent with previous study showing that the filtration flux halved during SFDM formation stage [23]. The final stabilized flux could be maintained at 30–50 LMH, which was higher than the reported results of 4.2–16 LMH [36]. For most filtration cycles, it was noted that the flux recovery after physical cleaning was nearly 100%, indicating a combined physical cleaning (air backwashing plus surface brushing) could be effective in membrane cleaning for SFDM regeneration [37].

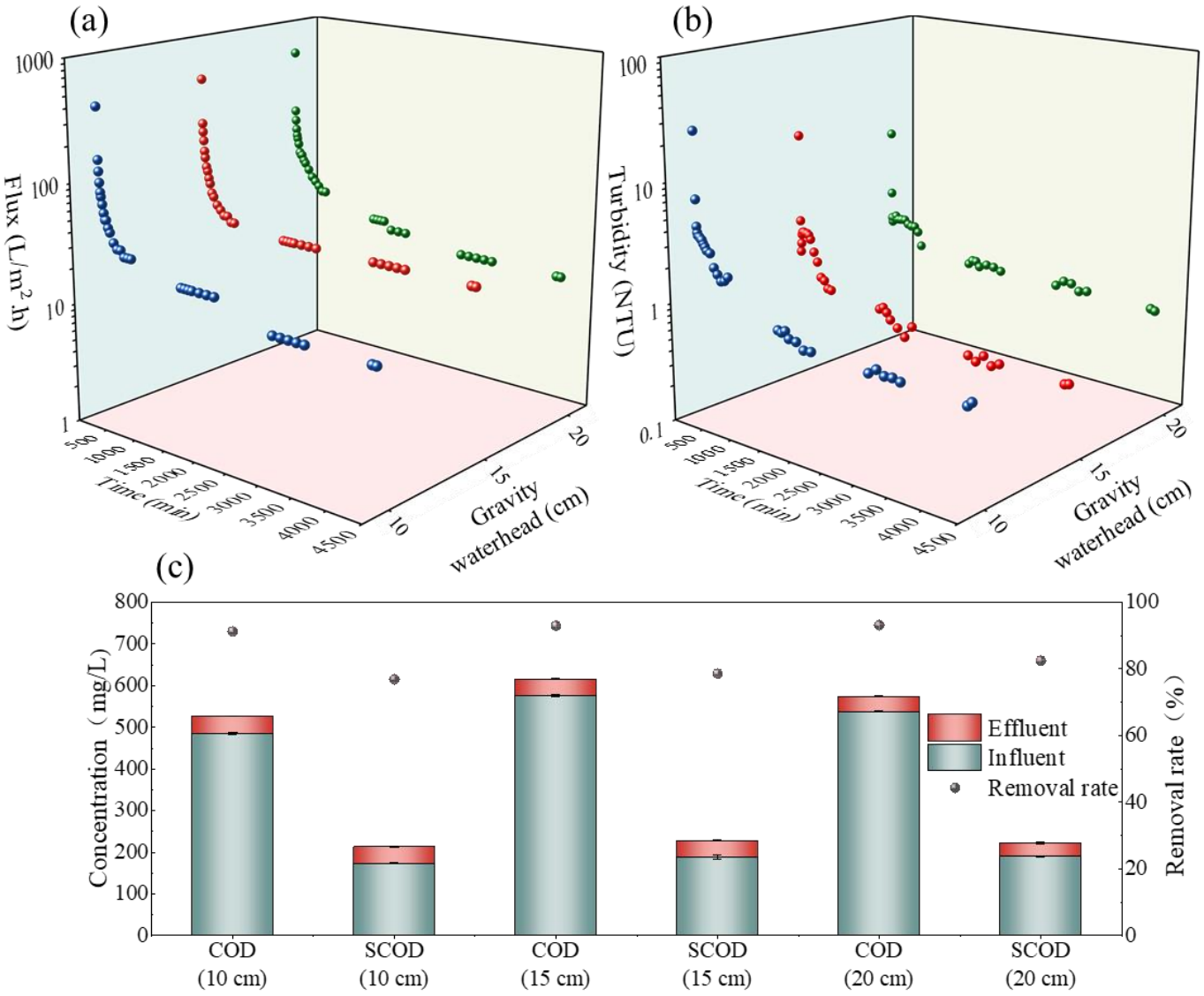


**Figure 6.** Filtration performance and COD removal under different gravity waterheads (10, 15, and 20 cm): (**a**) filtration flux; (**b**) effluent turbidity; (**c**) COD and SCOD removal.

The average influent turbidity was 148 NTU at the initial stage. In each filtration cycle, the effluent turbidity could drop to less than 2 NTU within 5 min. With the prolonged filtration time, the effluent turbidity further decreased to approximately 1 NTU in about 30 min. And thereafter, the effluent turbidity maintained in a low level, indicating that the SFDM could be formed with 5 min under the optimized condition and the formed SFDM was stable in structure evidenced by stabilized flux and effluent turbidity.

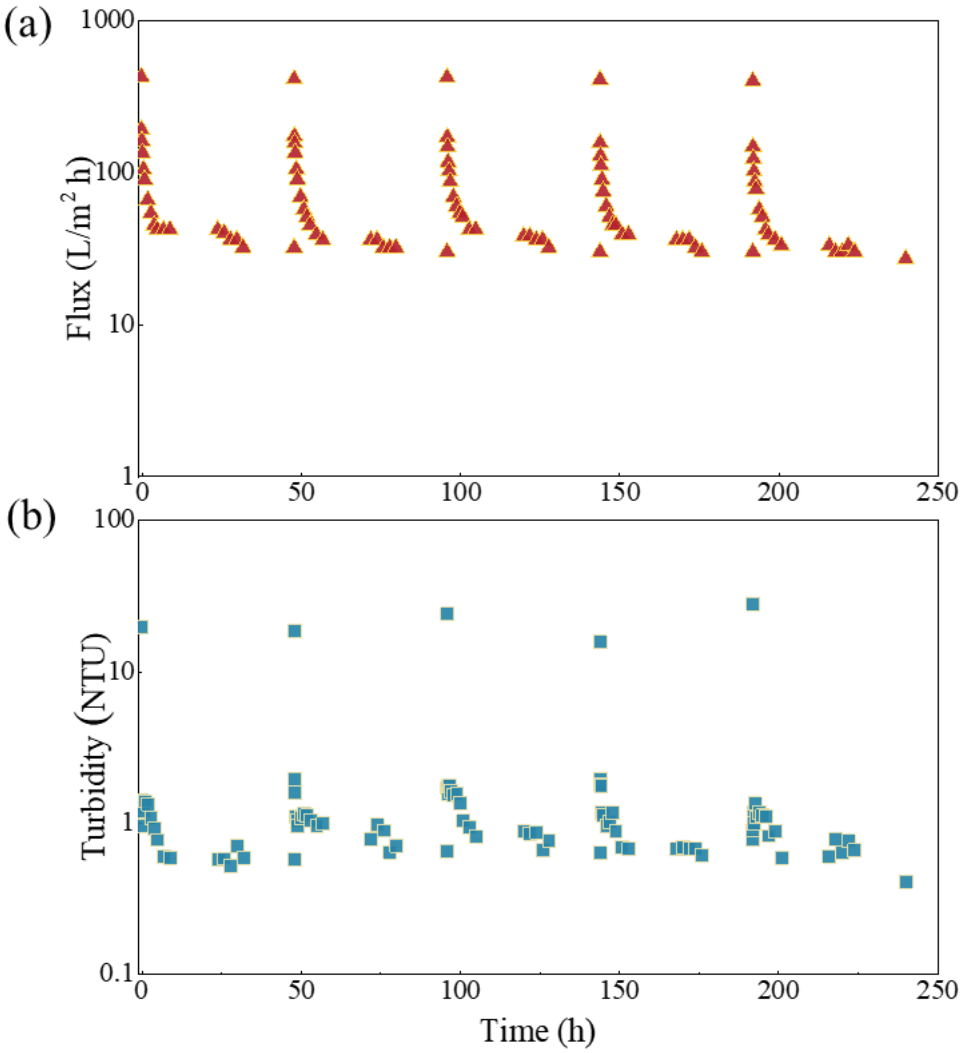


**Figure 7.** Filtration performance of the SFDMBR: (**a**) filtration flux and (**b**) effluent turbidity.

#### 3.5.2. Pollutants Removal Performance

In this study, the average concentrations of common pollutants (including COD, SCOD, $NH_4^+$-N, TN, and TP) in the influent and effluent as well as removal rates during continuous SFDMBR operation period were shown in Figure 8 (similar SFDMBR performance listed in Table S2). The results showed that the influent COD was 526.73 mg/L, and the effluent COD was 35.65 mg/L, and the removal efficiency of COD was as high as 93.28% on average. The retention effect of the efficiently formed SFDM and biodegradation both contributed to organics removal. Yang et al. [36] reported that the COD removal rate was 88%, but the removal rate of SCOD was only 68% in SFDMBR system. However, the COD removal in this investigation was as high as 82.58%, which might be because the more stable SFDM structure created under optimal conditions enhanced SCOD retention. The $NH_4^+$-N removal rate was as high as 95.46% due to the efficient nitrification process under the complete aerobic condition, whereas the removal rate of TN was only 21.83%, limited by negligible denitrification effect. Similarly, in this SFDMBR, about 21.83% of TP was removed mainly due to microbial assimilation [38].

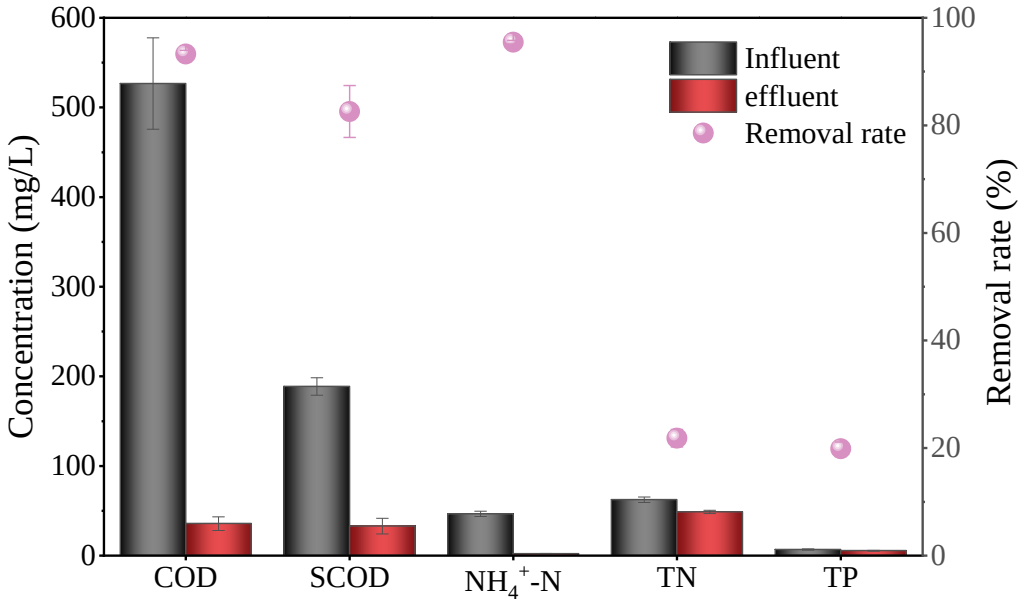


**Figure 8.** Common pollutants removal of SFDMBR under optimized SFDM formation conditions.

3.5.3. Properties of the Dynamic Membrane

Photographs of membrane modules, and SEM images and EDX analysis of pristine mesh and SFDM layer under optimized conditions were shown in Figure 9a. The yellow-brown sludge layer on the surface of the supporting material of the membrane module at the end of one operation cycle could be visualized, indicating the effective formation of SFDM. The thickness of this cake layer was determined to be 1.5 mm, so it could effectively retain the particulate matter and provide sufficient biodegradation of entrapped pollutants. The SEM images showed that the pristine membrane was distributed with even and clear micropores. Sludge particles and microbial cells could be observed in the SFDM [13]. Moreover, the morphology of the SFDM was rough and porous, thus the SFDM formed under the optimized conditions could maintain a high and stable flux.

The inorganic elements of pristine mesh and SFDM were revealed by EDX analysis. The following elemental composition was detected in the SFDM, and the relative weight percentages of the elementals were presented as follows: 47.11% C, 10.07% N, 17.48 O, 0.37% Mg, 0.18% Na, 0.22% Al, 1.15% Si, 5.59% P, 3.03% S, 1.51% Cl, 0.92% K, 3.78% Ca, 3.32% Cr, and 6.28% Fe. The relative content of the elements of C, N, and O was close to the molecular formula of microbial cells ($C_5H_7O_2N$) and the molecular formula of proteins ($C_{16}H_{24}O_5N_4$) according to a previous study [13]. This might indicate that the SFDM layer consists mainly of microorganisms and microbial metabolites. According to the previous work, although the contents of some metal elements (e.g., Mg, Al, Fe and Ca) accounted for a relatively small percentage, they could bridge the biopolymers and deposited microbes enhancing the formation of cake layer [39,40]. Further analysis of SFDM composition using FTIR analysis was carried out to reveal the main functional groups of the organic matter in the SFDM (Figure 9b). The peaks at 2974 $cm^{-1}$ and 2979 $cm^{-1}$ corresponded to C-H stretching. The peaks at 1660 $cm^{-1}$, 1546 $cm^{-1}$, 1388 $cm^{-1}$, and 1231 $cm^{-1}$ corresponded to amide I, amide II, and amide III, respectively [41]. And the peak at 1066 $cm^{-1}$ corresponded to the C-O stretching of PS or PS-like substances [42]. The stretching of these peaks further indicates that the main organic components in the SFDM layer are PN and PS.

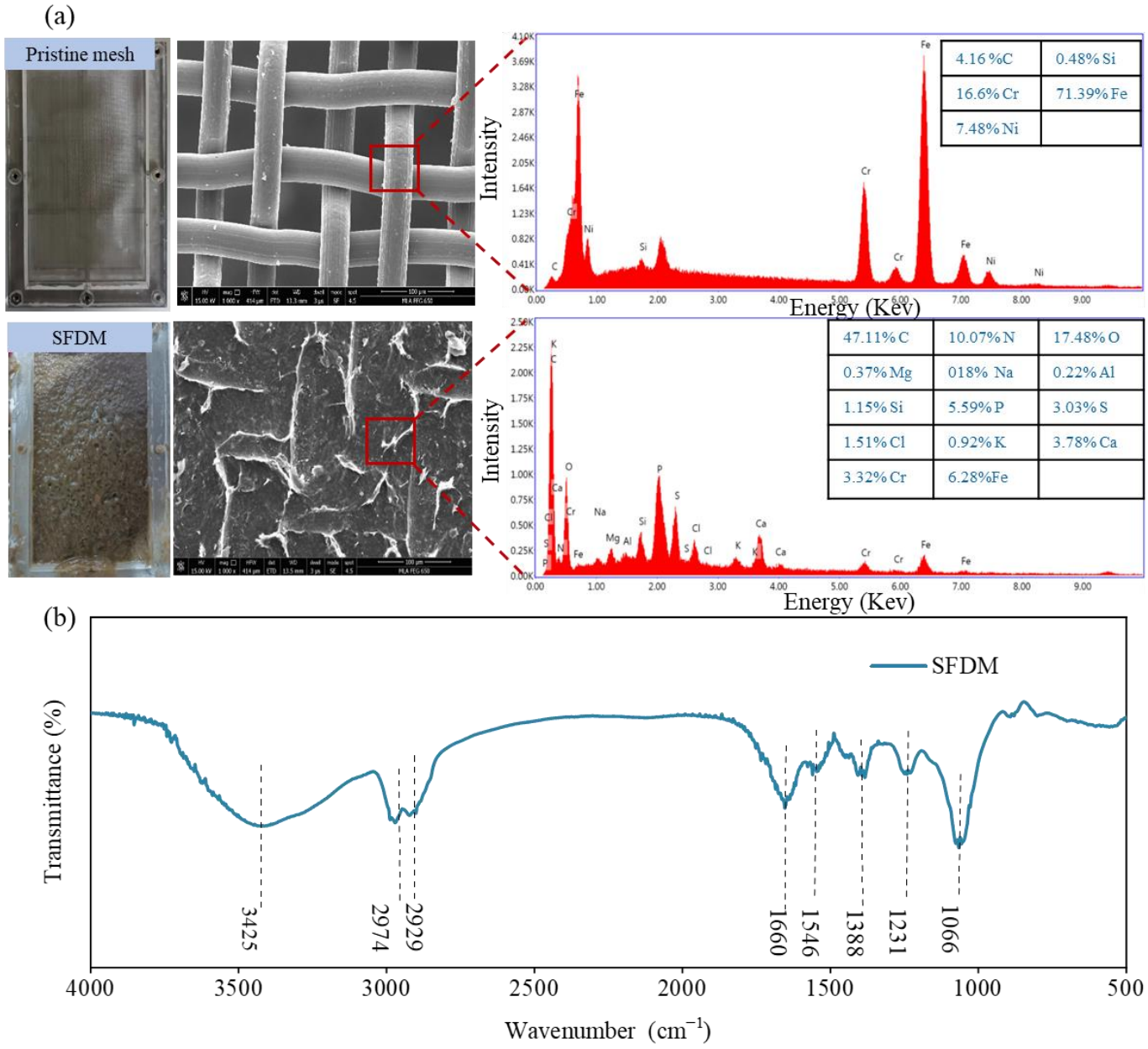


**Figure 9.** (**a**) SEM images and EDX analysis; pristine mesh and SFDM; (**b**) FTIR spectrum of SFDM.

The filtration resistance distribution of SFDM was further analyzed, as shown in Table 1. The total filtration resistance ($R_t$) of SFDM was calculated to be $1.72 \times 10^{11}$ m$^{-1}$ at the end of filtration cycle, and this value was one to three orders of magnitude lower than those commonly observed in conventional MBRs ($10^{12}$–$10^{14}$ m$^{-1}$) [43]. The intrinsic resistance ($R_m$) of the stainless-steel mesh (pore size of 48 µm) was $4.5 \times 10^9$ m$^{-1}$, which accounted for 1.33% of the total filtration resistance. Furthermore, the cake layer resistance ($R_c$) was $1.65 \times 10^{11}$ m$^{-1}$, accounting for 95.93% of the total resistance, with pore blocking resistance ($R_p$) of $0.47 \times 10^{10}$ m$^{-1}$ which was far less than the cake layer resistance. It meant that cake layer resistance was the major filtration resistance and membrane flux could be effectively restored only by simple physical cleaning due to the reversible nature of cake layer, and the pore resistance contributing much to filtration resistance in the MBRs could be effectively avoided in the SFDMBRs. It is worth noting that the SFDMBR showing lower filtration resistance and higher permeability is easy to clean compared with the MBR, but the membrane fouling cannot be avoided after a long-term operation. Thus, mitigating

SFDM fouling using low-cost physical cleaning methods need to be subsequently explored and optimized using advanced techniques like artificial intelligence.

**Table 1.** Filtration resistance distribution of the SFDMBR.

| | Intrinsic Resistance ($R_m$) | Cake Resistance ($R_c$) | Pore Blocking Resistance ($R_p$) | Total Resistance ($R_t$) |
|---|---|---|---|---|
| R ($\times 10^{10}$ $m^{-1}$) | 0.45 | 16.5 | 0.47 | 17.2 |
| Percentage (%) | 1.33 | 95.93 | 2.74 | 100 |

## 4. Conclusions

The SFDM could be efficiently formed within 5 min under the optimized formation condition, namely stainless-steel mesh with the pore size of 48 μm under MLSS concentration of 5–6 g/L and a gravity waterhead of 15 cm. Porous SFDM with a thickness of 1.5 mm formed under optimized conditions, allowing for efficient filtration performance and pollutants removal at a high steady-state filtration flux (30–50 LMH). Additionally, near 100% cake layer resistance indicated that the flux can be efficiently restored via simple physical cleaning methods. These results provided a helpful reference for the development and application of the low-cost SFDMBR process with limited maintenance requirement. Towards large-scale applications of the SFDMBR, artificial intelligence (such as machine learning methods) might be used to further analyze the SFDM filtration process and to optimize the SFDM formation conditions and fouling mitigation strategies.

**Supplementary Materials:** The following supporting information can be downloaded at: https://www.mdpi.com/article/10.3390/w15223963/s1. Table S1: A nomenclature list; Table S2: Operational performance comparison of SFDMBRs.

**Author Contributions:** L.T.: funding acquisition, writing-review and editing; J.Z.: funding acquisition, writing-review and editing; L.Z.: Investigation, writing-original draft operation, software; Y.H.: Conceptualization, supervision, writing-review and editing, funding acquisition, Y.Y. (Yiming Yang): writing-review and editing; Y.Z.: writing-review and editing; X.D.: writing-review and editing; Z.W. writing-review and editing; W.D.: software; Y.Y. (Yuan Yang): investigation. All authors have read and agreed to the published version of the manuscript.

**Funding:** This work was supported by the Natural Science Foundation of the Shaanxi Province (grant no. 2022JM-237), the China Postdoctoral Science Foundation (grant no. 2021MD703870) and the Shaanxi Provincial Program for Innovative Research Team (no. 2019TD-025).

**Data Availability Statement:** The data that supported the findings of this study are available from the corresponding author upon reasonable request.

**Conflicts of Interest:** The authors Luhe Tang, Jingyu Zhang, Yiming Yang, Yunsheng Zhao, Xinglong Dong, Zhanjiu Wang were employed by the Beijing Huayu Brilliant Eco-Environmental Protection Technology company. And remaining authors declare that the research was conducted in the absence of any commercial or financial relationships that could be construed as a potential conflict of interest.

## References

1. Meng, F.; Zhang, S.; Oh, Y.; Zhou, Z.; Shin, H.S.; Chae, S.R. Fouling in Membrane Bioreactors: An Updated Review. *Water Res.* **2017**, *114*, 151–180. [CrossRef] [PubMed]
2. Nguyen, M.L.; Nakhjiri, A.T.; Kamal, M.; Mohamed, A.; Algarni, M.; Yu, S.T.; Wang, F.M.; Su, C.H. State-of-the-Art Review on the Application of Membrane Bioreactors for Molecular Micro-Contaminant Removal from Aquatic Environment. *Membranes* **2022**, *12*, 429. [CrossRef] [PubMed]
3. Meng, F.; Chae, S.R.; Shin, H.S.; Yang, F.; Zhou, Z. Recent Advances in Membrane Bioreactors: Configuration Development, Pollutant Elimination, and Sludge Reduction. *Environ. Eng. Sci.* **2012**, *29*, 139–160. [CrossRef]
4. Zhang, J.; Xiao, K.; Huang, X. Full-Scale MBR Applications for Leachate Treatment in China: Practical, Technical, and Economic Features. *J. Hazard. Mater.* **2020**, *389*, 122138. [CrossRef]
5. Marjani, A.; Taghvaie Nakhjiri, A.; Adimi, M.; Fathinejad Jirandehi, H.; Shirazian, S. Modification of Polyethersulfone Membrane Using MWCNT-NH2 Nanoparticles and Its Application in the Separation of Azeotropic Solutions by Means of Pervaporation. *PLoS ONE* **2020**, *15*, e0236529. [CrossRef]

6. Liu, Q.; Ren, J.; Lu, Y.; Zhang, X.; Roddick, F.A.; Fan, L.; Wang, Y.; Yu, H.; Yao, P. A Review of the Current In-Situ Fouling Control Strategies in MBR: Biological versus Physicochemical. *J. Ind. Eng. Chem.* **2021**, *98*, 42–59. [CrossRef]
7. Chen, C.; Sun, M.; Chang, J.; Liu, Z.; Zhu, X.; Xiao, K.; Song, G.; Wang, H.; Liu, G.; Huang, X. Unravelling Temperature-Dependent Fouling Mechanism in a Pilot-Scale Anaerobic Membrane Bioreactor via Statistical Modelling. *J. Memb. Sci.* **2022**, *644*, 120145. [CrossRef]
8. Ersahin, M.E.; Ozgun, H.; Dereli, R.K.; Ozturk, I.; Roest, K.; van Lier, J.B. A Review on Dynamic Membrane Filtration: Materials, Applications and Future Perspectives. *Bioresour. Technol.* **2012**, *122*, 196–206. [CrossRef]
9. Wu, Y.; Huang, X.; Wen, X.; Chen, F. Function of Dynamic Membrane in Self-Forming Dynamic Membrane Coupled Bioreactor. *Water Sci. Technol.* **2005**, *51*, 107–114. [CrossRef]
10. Sahinkaya, E.; Yurtsever, A.; Çınar, Ö. Treatment of Textile Industry Wastewater Using Dynamic Membrane Bioreactor: Impact of Intermittent Aeration on Process Performance. *Sep. Purif. Technol.* **2017**, *174*, 445–454. [CrossRef]
11. Fan, B.; Huang, X. Characteristics of a Self-Forming Dynamic Membrane Coupled with a Bioreactor for Municipal Wastewater Treatment. *Environ. Sci. Technol.* **2002**, *36*, 5245–5251. [CrossRef] [PubMed]
12. Mohan, S.M.; Nagalakshmi, S. A Review on Aerobic Self-Forming Dynamic Membrane Bioreactor: Formation, Performance, Fouling and Cleaning. *J. Water Process Eng.* **2020**, *37*, 101541. [CrossRef]
13. Yang, Y.; Deng, W.; Zhang, J.; Dzakpasu, M.; Chen, R.; Wang, X.C.; Hu, Y. A Novel Precoated Anaerobic Dynamic Membrane Bioreactor for Real Domestic Wastewater Treatment: In-Situ Formation, Filtration Performance and Characterization of Dynamic Membrane. *Chem. Eng. J.* **2023**, *466*, 143313. [CrossRef]
14. Loderer, C.; Wörle, A.; Fuchs, W. Influence of Different Mesh Filter Module Configurations on Effluent Quality and Long-Term Filtration Performance. *Environ. Sci. Technol.* **2012**, *46*, 3844–3850. [CrossRef]
15. Ersahin, M.E.; Tao, Y.; Ozgun, H.; Gimenez, J.B.; Spanjers, H.; van Lier, J.B. Impact of Anaerobic Dynamic Membrane Bioreactor Configuration on Treatment and Filterability Performance. *J. Memb. Sci.* **2017**, *526*, 387–394. [CrossRef]
16. Ji, J.; Sakuma, S.; Ni, J.; Chen, Y.; Hu, Y.; Ohtsu, A.; Chen, R.; Cheng, H.; Qin, Y.; Hojo, T.; et al. Application of Two Anaerobic Membrane Bioreactors with Different Pore Size Membranes for Municipal Wastewater Treatment. *Sci. Total Environ.* **2020**, *745*, 140903. [CrossRef]
17. Saleem, M.; Masut, E.; Spagni, A.; Lavagnolo, M.C. Exploring Dynamic Membrane as an Alternative for Conventional Membrane for the Treatment of Old Landfill Leachate. *J. Environ. Manag.* **2019**, *246*, 658–667. [CrossRef]
18. Guan, D.; Dai, J.; Watanabe, Y.; Chen, G. Changes in the Physical Properties of the Dynamic Layer and Its Correlation with Permeate Quality in a Self-Forming Dynamic Membrane Bioreactor. *Water Res.* **2018**, *140*, 67–76. [CrossRef]
19. Sabaghian, M.; Mehrnia, M.R.; Esmaieli, M.; Noormohammadi, D. Formation and Performance of Self-Forming Dynamic Membrane (SFDM) in Membrane Bioreactor (MBR) for Treating Low-Strength Wastewater. *Water Sci. Technol.* **2018**, *78*, 904–912. [CrossRef]
20. Chu, L.; Li, S. Filtration Capability and Operational Characteristics of Dynamic Membrane Bioreactor for Municipal Wastewater Treatment. *Sep. Purif. Technol.* **2006**, *51*, 173–179. [CrossRef]
21. Hu, Y.; Wang, X.C.; Tian, W.; Ngo, H.H.; Chen, R. Towards Stable Operation of a Dynamic Membrane Bioreactor (DMBR): Operational Process, Behavior and Retention Effect of Dynamic Membrane. *J. Memb. Sci.* **2016**, *498*, 20–29. [CrossRef]
22. Nepa, C. *Water and Wastewater Monitoring Methods*, 4th ed.; Chinese Environmental Science Publishing House: Beijing, China, 2002.
23. Hu, Y.; Yang, Y.; Wang, X.C.; Hao Ngo, H.; Sun, Q.; Li, S.; Tang, J.; Yu, Z. Effects of Powdered Activated Carbon Addition on Filtration Performance and Dynamic Membrane Layer Properties in a Hybrid DMBR Process. *Chem. Eng. J.* **2017**, *327*, 39–50. [CrossRef]
24. Zhang, X.; Wang, Z.; Wu, Z.; Lu, F.; Tong, J.; Zang, L. Formation of Dynamic Membrane in an Anaerobic Membrane Bioreactor for Municipal Wastewater Treatment. *Chem. Eng. J.* **2010**, *165*, 175–183. [CrossRef]
25. Li, L.; Xu, G.; Yu, H.; Xing, J. Dynamic Membrane for Micro-Particle Removal in Wastewater Treatment: Performance and Influencing Factors. *Sci. Total Environ.* **2018**, *627*, 332–340. [CrossRef]
26. Cai, D.; Huang, J.; Liu, G.; Li, M.; Yu, Y.; Meng, F. Effect of Support Material Pore Size on the Filtration Behavior of Dynamic Membrane Bioreactor. *Bioresour. Technol.* **2018**, *255*, 359–363. [CrossRef]
27. Meng, Z.G.; Yang, F.L.; Zhang, X.W. MBR Focus: Do Nonwovens Offer a Cheaper Option? *Filtr. Sep.* **2005**, *42*, 28–30. [CrossRef]
28. Liang, S.; Qu, L.; Meng, F.; Han, X.; Zhang, J. Effect of Sludge Properties on the Filtration Characteristics of Self-Forming Dynamic Membranes (SFDMs) in Aerobic Bioreactors: Formation Time, Filtration Resistance, and Fouling Propensity. *J. Memb. Sci.* **2013**, *436*, 186–194. [CrossRef]
29. Zahid, W.M.; El-Shafai, S.A. Use of Cloth-Media Filter for Membrane Bioreactor Treating Municipal Wastewater. *Bioresour. Technol.* **2011**, *102*, 2193–2198. [CrossRef]
30. Chang, W.K.; Hu, A.Y.J.; Horng, R.Y.; Tzou, W.Y. Membrane Bioreactor with Nonwoven Fabrics as Solid-Liquid Separation Media for Wastewater Treatment. *Desalination* **2007**, *202*, 122–128. [CrossRef]
31. Wang, C.; Chen, W.N.; Hu, Q.Y.; Ji, M.; Gao, X. Dynamic Fouling Behavior and Cake Layer Structure Changes in Nonwoven Membrane Bioreactor for Bath Wastewater Treatment. *Chem. Eng. J.* **2015**, *264*, 462–469. [CrossRef]
32. Xiong, J.; Fu, D.; Singh, R.P. Self-Adaptive Dynamic Membrane Module with a High Flux and Stable Operation for the Municipal Wastewater Treatment. *J. Memb. Sci.* **2014**, *471*, 308–318. [CrossRef]

33. Poostchi, A.A.; Mehrnia, M.R.; Rezvani, F.; Sarrafzadeh, M.H. Low-Cost Monofilament Mesh Filter Used in Membrane Bioreactor Process: Filtration Characteristics and Resistance Analysis. *Desalination* **2012**, *286*, 429–435. [CrossRef]
34. Rezvani, F.; Mehrnia, M.R.; Poostchi, A.A. Optimal Operating Strategies of SFDM Formation for MBR Application. *Sep. Purif. Technol.* **2014**, *124*, 124–133. [CrossRef]
35. Wang, Y.K.; Sheng, G.P.; Li, W.W.; Yu, H.Q. A Pilot Investigation into Membrane Bioreactor Using Mesh Filter for Treating Low-Strength Municipal Wastewater. *Bioresour. Technol.* **2012**, *122*, 17–21. [CrossRef] [PubMed]
36. Yang, Y.; Deng, W.; Hu, Y.; Chen, R.; Wang, X.C. Gravity-Driven High Flux Filtration Behavior and Microbial Community of an Integrated Granular Activated Carbon and Dynamic Membrane Bioreactor for Domestic Wastewater Treatment. *Sci. Total Environ.* **2022**, *825*, 153930. [CrossRef] [PubMed]
37. Chu, H.; Cao, D.; Dong, B.; Qiang, Z. Bio-Diatomite Dynamic Membrane Reactor for Micro-Polluted Surface Water Treatment. *Water Res.* **2010**, *44*, 1573–1579. [CrossRef]
38. Kimura, K.; Nishisako, R.; Miyoshi, T.; Shimada, R.; Watanabe, Y. Baffled Membrane Bioreactor (BMBR) for Efficient Nutrient Removal from Municipal Wastewater. *Water Res.* **2008**, *42*, 625–632. [CrossRef]
39. Higgins, M.J.; Novak, J.T. Characterization of Exocellular Protein and Its Role in Bioflocculation. *J. Environ. Eng.* **1997**, *123*, 479–485. [CrossRef]
40. Gao, W.J.; Leung, K.T.; Qin, W.S.; Liao, B.Q. Effects of Temperature and Temperature Shock on the Performance and Microbial Community Structure of a Submerged Anaerobic Membrane Bioreactor. *Bioresour. Technol.* **2011**, *102*, 8733–8740. [CrossRef]
41. Gao, W.J.; Lin, H.J.; Leung, K.T.; Schraft, H.; Liao, B.Q. Structure of Cake Layer in a Submerged Anaerobic Membrane Bioreactor. *J. Memb. Sci.* **2011**, *374*, 110–120. [CrossRef]
42. Subtil, E.L.; Almeria Ragio, R.; Lemos, H.G.; Scaratti, G.; García, J.; Le-Clech, P. Direct Membrane Filtration (DMF) of Municipal Wastewater by Mixed Matrix Membranes (MMMs) Filled with Graphene Oxide (GO): Towards a Circular Sanitation Model. *Chem. Eng. J.* **2022**, *441*, 136004. [CrossRef]
43. Meng, F.; Chae, S.R.; Drews, A.; Kraume, M.; Shin, H.S.; Yang, F. Recent Advances in Membrane Bioreactors (MBRs): Membrane Fouling and Membrane Material. *Water Res.* **2009**, *43*, 1489–1512. [CrossRef] [PubMed]


**Disclaimer/Publisher's Note:** The statements, opinions and data contained in all publications are solely those of the individual author(s) and contributor(s) and not of MDPI and/or the editor(s). MDPI and/or the editor(s) disclaim responsibility for any injury to people or property resulting from any ideas, methods, instructions or products referred to in the content.